Indonesian Journal of Computing, Engineering, and Design

Journal homepage: http://ojs.sampoernauniversity.ac.id/index.php/IJOCED

Behavior of Grouted Sleeve Wall Connection under Lateral Load

Jen Hua Ling[1], Ahmad Baharuddin Abd. Rahman[2], Izni Syahrizal Ibrahim[2]*

[1] Centre for Research of Innovation & Sustainable Development, School of Engineering and Technology, University of Technology Sarawak, 96000 Sarawak, Malaysia

[2] School of Civil Engineering, Faculty of Engineering, Universiti Teknologi Malaysia, 81310 Skudai, Johor Darul Ta'zim, Malaysia

Corresponding email: lingjenhua@uts.edu.my

ABSTRACT

A grouted sleeve's efficiency in splicing steel bars makes it a potential choice for connecting precast elements. While most studies have focused on the feasibility of grouted sleeves under tension, only a few have investigated the real response of precast concrete members connected using grouted sleeves. In this study, Tapered Head Sleeves (THS) were utilized as connections for precast walls. The objectives were to examine their behavior under incremental lateral loads and assess the feasibility of THS as a wall connection. Five test specimens and one control specimen were fabricated, each comprising two walls joined by THS. The load was applied 1.8 m above the joint until specimen failure. Specimens that experienced bar fracture failure exhibited a relatively large drift upon failure, while those failing due to bar bond slip showed smaller drift. Factors contributing to wall drift included horizontal slip, rocking displacement, cantilever bending deformation, and compressive settlement. The ultimate load increased by 71% as the embedded length increased from 75 mm to 175 mm, and it increased by 50% as the sleeve diameter decreased from 75 mm to 50 mm. The sleeves' performance was evaluated for feasibility based on the strength ratio, drift ratio, ductility ratio, failure mode, performance ratio, serviceability ratio, and length ratio. Only THS-8 met all the criteria, suggesting that the bar's embedded length should be at least 11 times the bar diameter.

ARTICLE INFO

Article History:
Received 01 Jan 2023
Revised 11 Jan 2024
Accepted 24 Feb 2024
Available online 01 Apr 2024

Keywords:
Feasibility study,
Flexural loads,
Grouted sleeve,
Precast wall connection,
Splicing bars.

1. INTRODUCTION

Precast concrete walls are structural systems made up of factory-prefabricated panels. It is commonly used in building construction, offering the benefits of shorter construction time, less labor, less

energy usage, and better-quality control (Zheng et al., 2018; Lu et al., 2019; Lin and Zhao, 2020). The structure relies heavily on the connection for structural integrity and stability (Li et al., 2022).

Grouted sleeves can be used to join precast walls. It consists of a sleeve and grout. The sleeves implanted in a wall are used to splice the steel bars extruded from another wall. The grout bonds with the bars, preventing them from being pulled out (Sun et al., 2021; Ling, 2011). The sleeve confines the grout and limits the lateral expansion (Ling et al., 2022). It controls the splitting cracks and enhances the bond (Untrauer and Henry, 1965; Moosavi et al., 2005; Ling et al., 2012; Ling et al., 2016; Einea et al., 1995).

The bar's embedded length in grouted sleeves is typically shorter than the conventional bar-lapping system, ranging from 8.5 to 16 times the bar's diameter (Haber et al., 2015). Recent studies proposed even shorter lengths, ranging from 5 to 6.4 times the bar diameter (Wang et al., 2021; Huang et al., 2023; Lu et al., 2019).

Grouted sleeves can be made from various materials. This includes mild steel pipes (Einea et al., 1995; Henin and Morcous, 2015; Abd. Rahman et al., 2010; Ling et al., 2012; Alias et al., 2014; Alias et al., 2013; Lu et al., 2019; Zheng et al., 2018; Huang et al., 2023), high strength steel (Seo et al., 2016), cast iron (Xu et al., 2019), aluminium tubes (Ling et al., 2008; Tullini and Minghini, 2016), spirals (Aldin Hosseini and Abd. Rahman, 2013; Aldin Hosseini and Abd. Rahman, 2016; Aldin Hosseini et al., 2015; Sayadi et al., 2014; Hosseini and Rahman, 2013), square hollow sections (Ling et al., 2014) and glass fibre reinforced polymers (Sayadi et al., 2015; Koushfar 0065t al., 2014; Tastani, 2002; Tibbetts et al., 2009). The load-resisting mechanism, structural performance, and efficiency of different connectors vary substantially depending on the material properties and geometric parameters.

Researchers have studied variables like rebar diameter, grouted sleeve type, grouted compressive strength, rebar anchorage length, rebar tensile strength, and sleeve outer diameter-to-wall thickness ratio (Ma et al., 2023). Among the findings were: (a) tensile capacity increased with rebar diameter (Lu et al., 2019); (b) bond strength improved with higher grout compressive strength and increased rebar anchorage length (Ma et al., 2023); and (c) a bigger bar size required a greater bar's embedded length (Al-Jelawy, 2022).

Grouted sleeves generally perform well under tensile loads. The tensile strength is governed by (a) the tensile strength of the sleeve, (b) the bond strength between the grout and the spliced bar, (c) the bond strength between the grout and the sleeve, and (d) the tensile strength of the spliced bars, whichever is weaker (Abd. Rahman et al., 2010; Ling et al., 2014). This leads to failure modes of grouted sleeves like rebar fracture, rebar slip, grout slip, and sleeve fracture (Huang et al., 2023; Al-Jelawy, 2022; Abd. Rahman et al., 2010). A good, grouted sleeve should have a tensile strength greater than 1.25 times the spliced bar's nominal yield strength (ACI-318, 2008; AC-133, 2008).

Most studies tested grouted sleeves under tensile loads, focusing on assessing their feasibility as connectors for steel bars. However, few had tested them together with precast concrete members to evaluate their actual responses. The grouted sleeve's response under tension may not adequately represent the behavior of the precast members it connects, especially when forces other than tension is also involved.

Furthermore, a grouted sleeve may not be effective under a lateral load that

acts perpendicularly to it. The behavior would be distinct from that of a tensile load. Despite the pullout force, the grouted sleeve must also withstand the lateral load. Thus, it is vital to analyze the connector's behavior under lateral load.

This paper presents an experimental study carried out on a grouted sleeve known as the Tapered-Head Sleeve (THS). The connector was used to join precast walls that were subjected to lateral load. The objectives were to investigate the behavior of THS under incremental lateral load and to determine the feasibility of THS as a wall connection.

2. EXPERIMENTAL PROGRAM

2.1. Grouted Sleeve

Tapered-Head Sleeve (THS) was made of mild steel pipes, with a nominal yield strength of 250 N/mm^2. The pipe diameters were 50 mm, 65 mm, and 75 mm (**Figure 1** and **Table 1**). The length and thickness were 360 mm and 45 mm, respectively. The pipes were made into a tapered shape with an opening diameter of 35 mm at both ends.

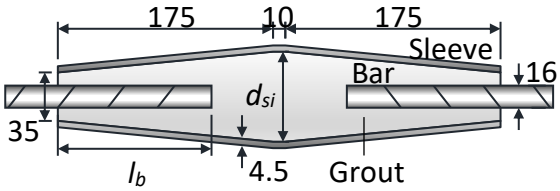

Figure 1. Tapered Head Sleeve (THS) (units in mm)

Table 1. Dimension of Tapered Head Sleeve (THS)

Specimen	Bar embedded length, l_b (mm)	Sleeve diameter, d_{si} (mm)
Control	-	-
THS-2	75	65
THS-4	125	50
THS-5	125	65
THS-6	125	75
THS-8	175	65

Steel bars of 16 mm in diameter were spliced in THS. The nominal yield strength of the bars was 500 N/mm^2. THS was used to splice the bars, which had embedded lengths of 75 mm, 125 mm, and 175 mm.

High-strength and non-shrink grout was used in THS. The grout had a nominal compressive strength of 70 N/mm^2. It was used in a pour-able state with a mixed proportion of 4 liters of water to 25 kg of grout. It was poured into the sleeve before the insertion of the steel bar.

2.2. Wall Assembly Specimen

Five test specimens and a control specimen were fabricated. Each specimen comprised two walls and a layer of drypack (**Figure 2**). Two THSs were embedded in the lower wall. The two steel bars extruding from the upper walls were then inserted into the THSs.

Both the upper and lower walls were (a) separately cast in the laboratory, (b) cured by using wet jute sacks and plastic sheets for 7 days, (c) vertically assembled after day 7, and (d) tested with lateral load after day 28.

The details of the specimen are:

- Load: horizontally applied at 1800 mm above the drypack
- Upper wall: 1200 mm (width) x 150 mm (thick) x 2100 mm (height)
- Lower wall: 1200 mm (width) x 150 mm (thick) x 600 mm (height)
- Reinforcements in both walls: 2 layers of Y10-200 in both directions (nominal yield strength = 500 N/mm^2)
- Spliced bars: Y16 (nominal yield strength = 500 N/mm^2)
- Concrete: Ready-mix concrete, Grade 40, slump 75 ± 25 mm, 20 mm crushed aggregate
- Drypack: 25 mm thickness, cement-to-sand ratio = 1:3
- Grout: *Sika Grout-215* (nominal compressive strength = 70 N/mm^2)
- Connection: 2 units of THS embedded in the lower wall

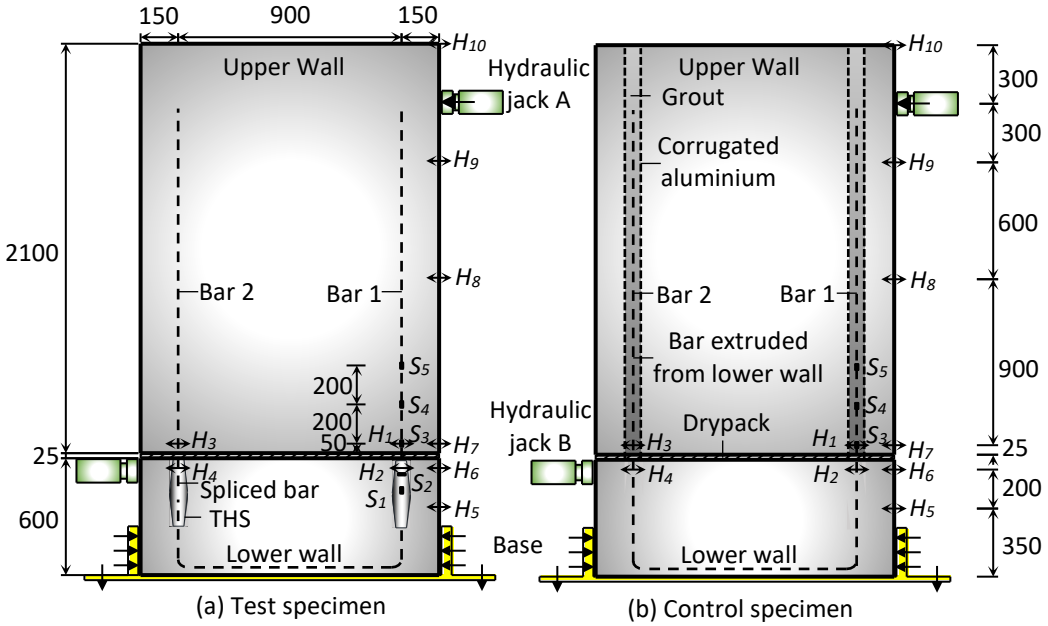

Figure 2. Details and instrumentation of wall specimens (units in mm)

2.3. Test Setup and Instrumentation

The equipment and instrumentation used include:

- two hydraulic jacks with a load capacity of 500 kN that applied forces to the specimen
- two load cells of 500 kN capacity that measured the load induced by the hydraulic jacks
- ten linear variable differential transducers (LVDT) that measured the displacement of the specimen
- five strain gauges that measured the strain of the sleeve and the spliced bar
- a data logger with 30 channels used for data acquisition
- a laptop used to monitor the data

The regional displacements of the specimen were measured by LVDTs H_1 to H_{10} (**Figure 2**). The differences between (a) H_1 and H_2, and (b) H_3 and H_4 resembled the horizontal displacements of the upper panel at the connection. H_5 and H_6 underlay the tilting movement of the entire specimen. H_7 to H_{10} measured the horizontal displacement of the upper wall at various heights. The strain gauges were installed along Bar 1: (**Figure 2**)

- S_1 was installed longitudinally at the mid-length of the sleeve to measure the elongation of the sleeve.
- S_2 was installed transversely on the sleeve at the midpoint of the embedding bar to measure lateral sleeve deformations caused by the splitting expansion of the grout in the sleeve (Einea *et al.*, 1995; Henin and Morcous, 2015)
- S_3 was installed on the spliced bar at 50 mm from the drypack to measure the bar's regional elongation (ASTM, 2005).
- S_4 was installed on the spliced bar at 200 mm from S_3 to measure the bar's regional elongation.
- S_5 was installed on the spliced bar at a 200 mm distance from S_4 to measure the bar's elongation.

2.4. Test Procedure

The test was conducted following ASTM E564 (2006). Before testing, all readings were initialized to zero. The specimen was preloaded to 10% of the estimated load capacity. The load was held for 5 minutes to consolidate the test setup. The load was then released for another 5

minutes for recovery. The process was repeated twice before the test started.

The load progressively increased in three cycles. It was held for 1 minute before the readings were taken. The load was slowly reduced upon reaching 1/3 and 2/3 of the estimated load capacity during the first two cycles. Readings were taken 5 minutes after the removal of the load. In the third load cycle, the specimen was tested until failure.

The test started with the load-controlled mode, with readings taken every 10 kN of load. At the later stage of the test, the drift-controlled mode was adopted, and readings were taken every 2 mm drift.

3. TEST RESULTS

3.1. Material Properties

Table 2 shows the compressive strengths of concrete, mortar, and grout. These materials were used in walls, drypack, and sleeves. The results were obtained from the cube samples tested alongside the wall specimens.

Table 2. Compressive strengths of concrete, mortar, and grout

Specimen	Compressive strength (N/mm^2)		
	Concrete	Mortar	Grout
Control	59.6	21.4	73.1
THS-2	71.2	27.0	96.1
THS-4	64.5	18.6	71.2
THS-5	62.6	29.4	77.8
THS-6	69.1	34.4	73.7
THS-8	67.4	23.1	85.9

Table 3 presents the properties of the steel bars used in the study. The main and secondary reinforcements in walls were Y10 bars, while THS was spliced with Y16 bars.

Table 3. Tensile strength of steel bars

Steel bar	Sample	Yield stress (N/mm^2)	Ultimate stress (N/mm^2)	Strain (%)
Y10	A	740	777	3.6
	B	722	814	4.3
	C	678	670	4.8
Y16	A	570	667	9.7
	B	571	663	10.8
	C	560	655	10.2

The quality of the materials was considered acceptable as:

- The concrete, mortar, and grout strengths were consistently greater than the required strengths of 40 N/mm^2, 20 N/mm^2, and 70 N/mm^2, respectively.
- All the steel samples met the nominal yield strength of 500 Nmm^2.

3.2. Load-Drift Response

Figure 3 shows the specimen conditions before and after testing. In the ultimate state, the upper panel was uplifted and tilted, causing horizontal drift in the direction of the lateral load. The uplift led to the detachment of the upper panel, drypack, and lower panel, resulting in large cracks at the construction joints.

Figure 4 and **Table 4** present the load-drift response of each specimen. The response was based on the horizontal displacement of the upper wall, where the lateral load was applied. The specimens resisted the load by having tensile stress in Bar 1 and compressive stress in Bar 2 and its surroundings. The tensile stress in Bar 1 created a pullout force on the grouted sleeve. The specimens' performance was governed by the ability of the connector to resist this pullout force.

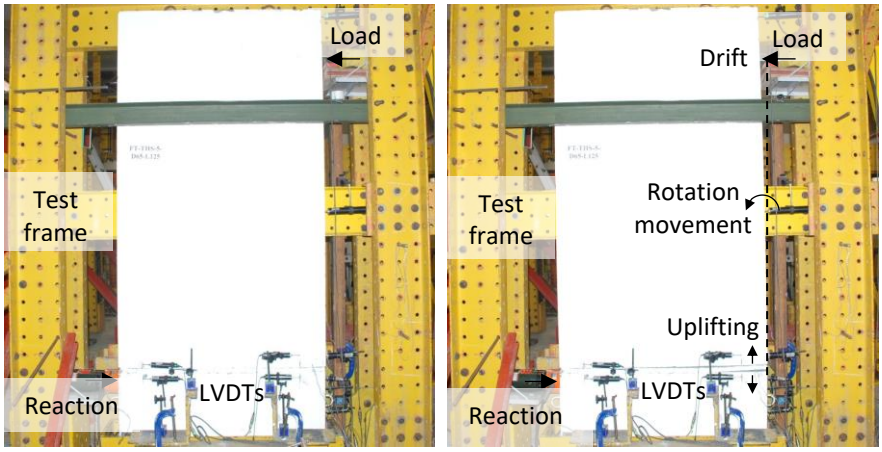

(a) Before testing (b) After testing

Figure 3. Response of specimen THS-5 before and after testing

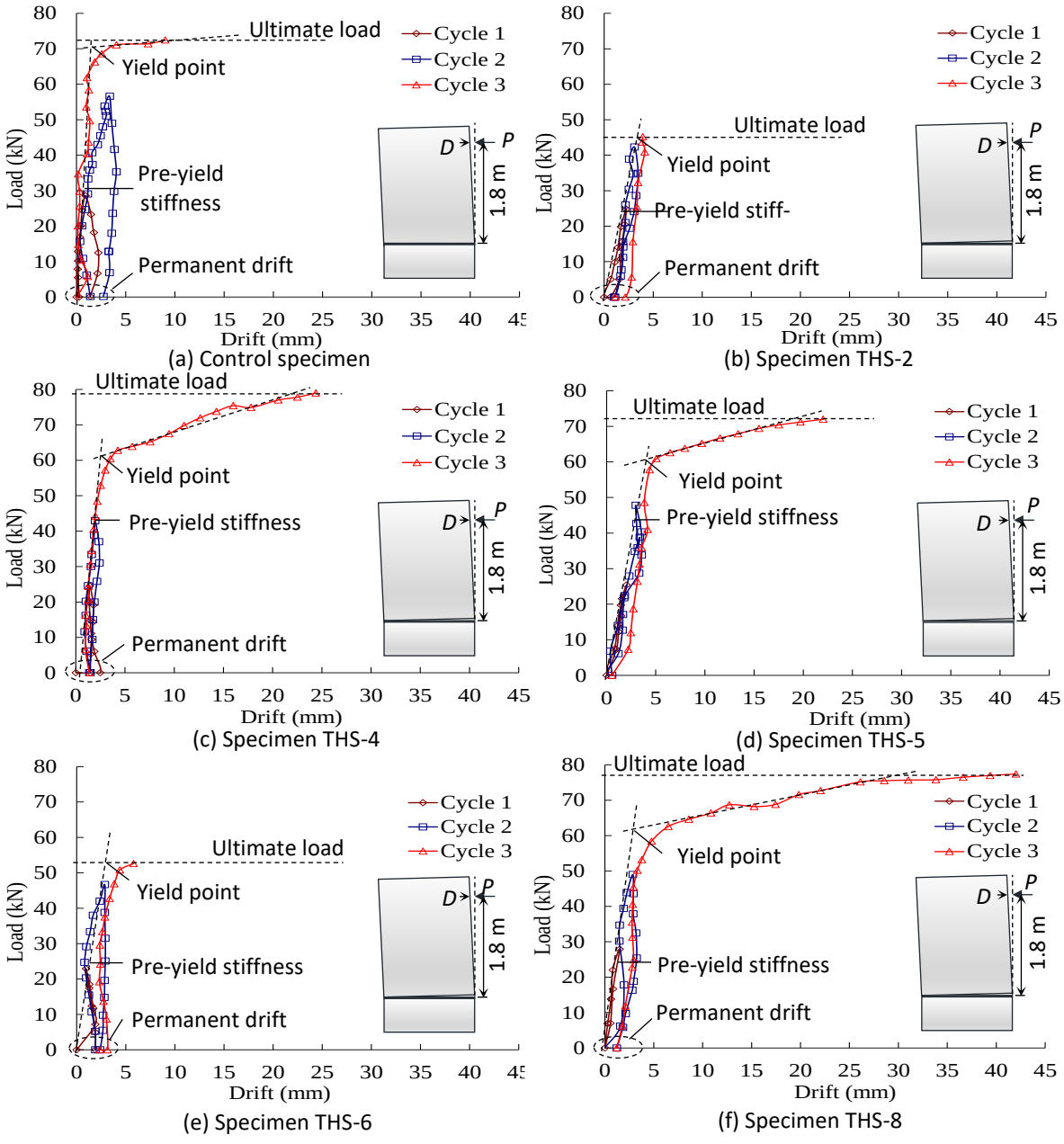

(a) Control specimen (b) Specimen THS-2

(c) Specimen THS-4 (d) Specimen THS-5

(e) Specimen THS-6 (f) Specimen THS-8

Figure 4. Load-drift response

Table 4. Compressive strengths of concrete, mortar, and grout

Specimen	Yield state		Ultimate state		Failure mode
	Yield load, P_y kN	Yield drift, δ_y (mm)	Ultimate load, P_u (kN)	Ultimate drift, δ_u (mm)	
Control			72.5	9.0	Failure of lower wall*
THS-2	45.2	3.78	45.2	4.0	Bond slip at bar 1
THS-4	62.7	3.16	79.0	24.4	Bond slip at bar 1
THS-5	61.8	4.89	72.0	22.0	Bond slip at bar 1
THS-6	52.6	4.07	52.6	5.8	Bond slip at bar 1
THS-8	64.0	4.14	77.4	42.0	Fracture at Bar 1

**The specimen failed prematurely due to excessive stress at the base that resisted the movement of the lower wall. The results did not represent the full capacity of the specimen.*

Two main types of responses were observed. Specimens THS-2 and THS-6 exhibited brittle failure. The upper walls of these specimens drifted slightly (not exceeding 5.8 mm) and failed suddenly. Specimens THS-4, THS-5, and THS-8 showed ductile behavior. The specimens drifted considerably (22 mm to 42 mm) before failure.

The concrete around the grouted sleeves was removed to assess the spliced bars' conditions. The spliced bars of specimens THS-2, THS-4, THS-5, and THS-6 slipped out of the grouted sleeve, while THS-8 experienced bar fracture (**Figure 5**). Notably, all failures occurred at bar 1 within the drypack area, as it was subjected to tension resisting the uplifting of the upper panel.

Table 5 highlights the role of the grouted sleeve bond strength in governing the response of the specimens. Specimens THS-2 and THS-6 demonstrated brittle bar bond-slip failure, with bond strength below the spliced bar's yield strength. THS-4 and THS-5 experienced bar bond-slip failure with some ductility, as their bond strength exceeded the yield strength but fell below the tensile strength of the spliced bar. Specimen THS-8, with bond strength surpassing both the yield and tensile strengths, exhibited failure by bar fracture with a high level of ductility.

Responding to the lateral loads, the specimens generally started with high stiffness (**Figure 4**). The load-drift curves were relatively steep initially. The upper walls drifted slowly as the load increased. The specimens showed close-to-elastic behavior before reaching the yield point. This was owing to (a) the strong bond in the grouted sleeve and (b) the elastic response of Bar 1 at the initial stage.

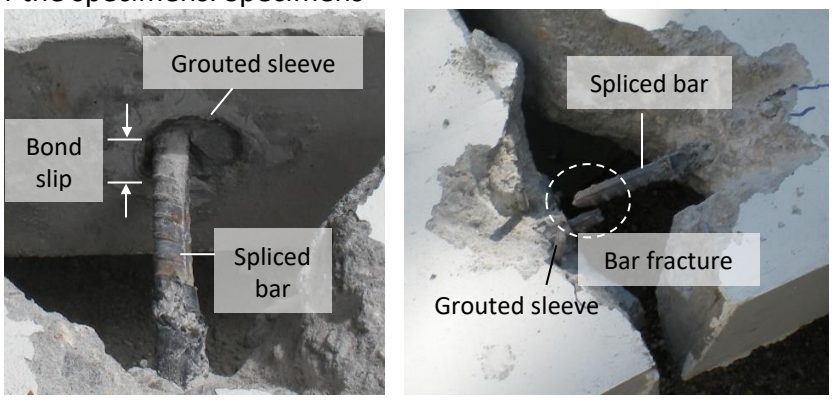

(a) Bar bond slip (THS-6) (b) Bar bond slip (THS-8)

Figure 5. Typical failure mode

Table 5. Comparison of specimens' response

Specimen	**THS-2 and THS-6**	**THS-4 and THS-5**	**THS-8**
Response	Brittle	Ductile	Ductile
Load capacity	Low	Moderate / High	High
Total displacement	Low	Moderate / High	High
Failure mode	Bond-slip of Bar 1	Bond-slip of Bar 1	Fracture of Bar 1
Characteristic	Failed suddenly. Post-yield stage (plastic response) was not noticeable or unclear.	Drifted significantly before failure. Post-yield stage (plastic response) was noticeable.	Drifted significantly before failure. Post-yield stage (plastic response) was noticeable.
Toughness	Low (small area below graph)	Moderate / High (large area below graph)	High (large area below graph)
Cause of failure	• Bond strength < yield strength of the spliced bar	• Bond strength > yield strength of the spliced bar • Bond strength < tensile strength of the spliced bar	• Bond strength > yield strength of the spliced bar • Bond strength > tensile strength of the spliced bar
Yield strength of the specimen	• Yield strength of specimen < yield strength of the spliced bar • Yield strength of specimen ≈ ultimate tensile capacity of the specimen	• Yield strength of specimen ≈ yield strength of the spliced bar • Yield strength of specimen < ultimate tensile capacity of the specimen	• Yield strength of specimen ≈ yield strength of the spliced bar • Yield strength of specimen < ultimate tensile capacity of the specimen

Specimens THS-4, THS-5, and THS-8 exhibited symptoms of yielding before ultimate failure. The stiffness started degrading at around 60 kN load. This was due to the yielding of Bar 1, which was counteracting the lateral load. After yielding, the bar experienced plastic deformation and elongated significantly. This subsequently accelerated the drift of the upper load.

Specimens THS-2, THS-4, THS-5, and THS-6 failed as Bar 1 slipped out of the sleeves. Their bar-embedded lengths were 125 mm or less, which was inadequate to generate sufficient bond strength to resist the pullout force. Among the specimens, THS-2 and THS-6 failed in a brittle manner. The ultimate capacities and drifts were relatively low. The bond strengths in the sleeve were insufficient to yield the spliced bars. On the other hand, THS-4 and THS-5 had bond strengths exceeding the yield strength of the spliced bars. This led to considerable plastic elongation of Bar 1. Thus, the specimens endured more drift before failure.

THS-8 failed due to a bar fracture. The bond strength in the sleeve exceeded the tensile capacity of the spliced bar. The 175 mm bar-embedded length was adequate to generate a sufficient bond to prevent the slippage of the bar. The spliced bar yielded and elongated significantly. This caused the specimen to drift significantly before failure.

3.3. Drift Response

The first and second load cycles ended at 25 kN and 50 kN, respectively. The lateral loads were released before the yield point of the specimens. Despite this, the specimens were unable to regain their original states. There were permanent

drifts not exceeding 3 mm (**Figure 4**). These permanent drifts were due to the non-recoverable deformations of specimens caused by the load.

Theoretically, the drift was due to the combined effects of (a) the horizontal slip, (b) the rocking displacement, (c) the cantilever bending deformation, and (d) the compressive settlement of the upper wall (**Figure 6** and **Table 6**). These components took place once the load was applied. The horizontal slip was not recoverable once the upper panel slid. The consolidation of cold joints was also not recoverable once it took place. This happened before the specimens reached the yield point. The permanent drifts at the end of the first two load cycles were believed to be due to these two components. The rocking displacement and the cantilever bending deformation would be permanent if Bar 1 and the reinforcements in the upper wall yielded.

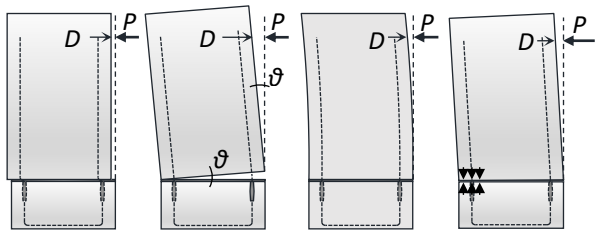

(a) Horizontal slip (b) Rocking displacement (c) Cantilever bending deformation (d) Compressive settlement

Figure 6. Factors contributing to wall drift

Table 6. Descriptions of the factors that contributed to wall drift

Components	Description	Factors influencing the magnitude	Recovery after load removal	
			Before yield point	After yield point*
Horizontal slip	• Horizontal displacement of the upper wall in the direction of the lateral load. • Triggered as the sliding force exceeded the frictional force at the joint	• the magnitude of the lateral load • the frictional resistance of the joint.	Not recoverable as the upper panel slid	Not recoverable
Rocking displacement	• Rotational movement of the upper wall due to the moment generated by the lateral load. • Increased with the elongation of Bar 1.	• the magnitude of the moment acting on the upper wall • the elasticity of Bar 1.	Recoverable	Not recoverable if Bar 1 yielded
Cantilever bending deformation	The bending deformation of the upper wall as a cantilever member.	• the magnitude of the moment acting on the upper wall, • the moment of inertia of the reinforced wall section.	Recoverable	Not recoverable if the reinforcements in the upper wall yielded.
Compressive settlement	Consolidation of cold joints	• the space between the drypack and walls • the compactness of drypack	Not recoverable after the consolidation.	Not recoverable
	Elastic shortening of the concrete, mortar drypack, and Bar 2 under compression.	• the magnitude of compressive stress, • the elastic modulus of the materials	Recoverable	Not recoverable if the strain limits of the materials were exceeded

**conditional to yielding or failure of the materials*

In this study, the upper and lower walls were quite heavily reinforced. No visible crack on the upper wall was observed throughout the test. The cantilever bending deformation would be quite minimal. Since the reinforcements in the upper wall did not yield, the drifts caused by this component should theoretically be recoverable if the load was released before the ultimate state. Similarly, no crushing of concrete or drypack was noticed. The elastic shortening of the materials should also be recoverable upon the removal of loads.

The load capacity increased notably when the bar embedded length in the sleeve increased. This can be seen in specimens THS-2, THS-5, and THS-8. As the bar embedded length increased from 75 mm to 175 mm, the ultimate load increased 71% from 45.2 kN to 77.4 kN.

On the other hand, the sleeve diameter also influenced the load capacity of the specimen. This was demonstrated by specimens THS-4, THS-5, and THS-6. When the sleeve diameter decreased from 75 mm to 50 mm, the load capacity increased by 50% from 52.6 kN to 79 kN.

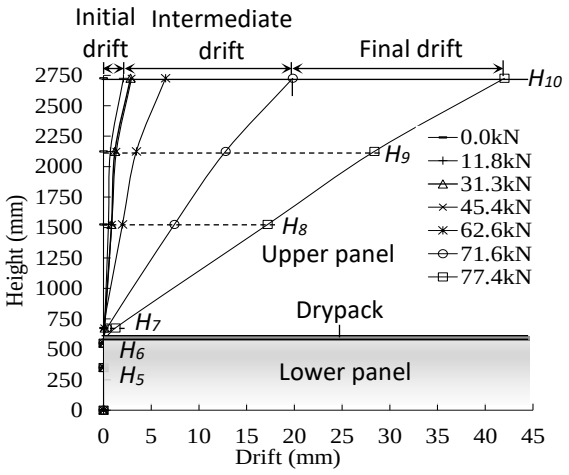

Figure 7. Typical drift profile of the upper wall at different load levels (THS-8)

Figure 7 shows the typical drift profile of the specimens under lateral load. The curves were based on the horizontal displacements of the upper wall at different heights, as measured by LVDTs H_5 to H_{10}. The displacement at the drypack joint was relatively small. Higher up from the joint, the displacement increased.

The drift developed quickly at the early stage as the load increased from 0 kN to 11.8 kN. This was mainly due to the consolidation of the joints of the walls when the lateral load was first applied. This was followed by a slow increase in drift after the consolidation. The drift increased marginally when the load increased from 11.8 kN to 31.3 kN. Due to the slight elongation of the spliced bar, small rocking displacements developed. After that, the spliced bar yielded and elongated significantly. This resulted in an accelerated drift after 45.4 kN. The drift was the highest in the ultimate state when THS failed.

The drift profile exhibited a non-linear curvature initially. Reaching the ultimate state, the curvature became relatively linear. In the beginning, the entire specimen resisted the lateral load with good integrity. The cantilever bending deformation was relatively high. After that, the spliced bar yielded and lost its stiffness. High stress was concentrated at Bar 1. As a result, the upper wall tilted and the cantilever bending deformation decreased.

3.4. Uplifting Response

Figure 8 shows a typical uplifting of the upper wall along the drypack joint. The overturning rotation of the upper wall caused by the lateral load led to (a) the uplifting of the upper wall, (b) the tensile elongation of Bar 1, (c) the tensile or compressive deformation of Bar 2, and (d) the compressive deformation of the drypack (**Figure 9**). Bar 2 was in compression when the lateral load was 26.4 kN. Reaching the ultimate state of around 72 kN, it transformed into tension.

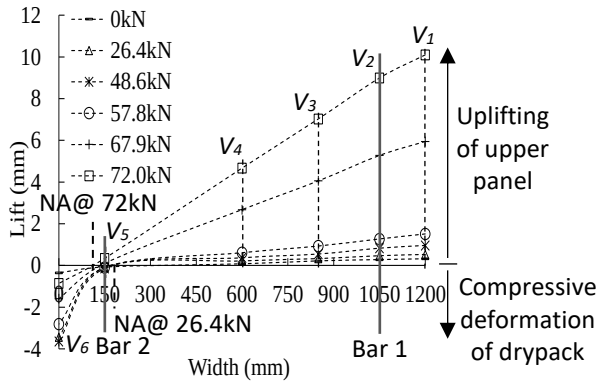

Figure 8. Typical uplifting profile of upper wall at different load levels (THS-5)

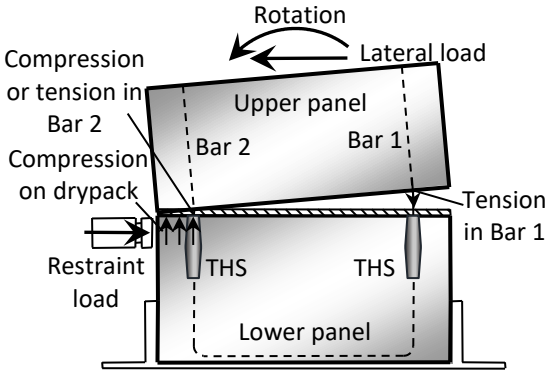

Figure 9. Uplifting response of the specimen

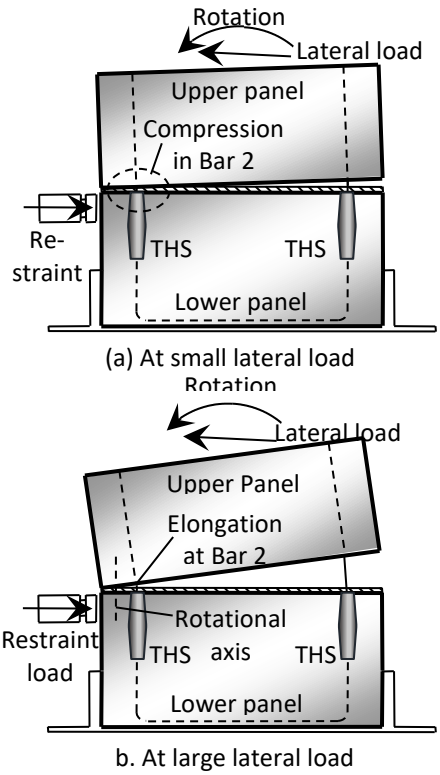

Figure 10. The neutral axis of rotation shifted with the flexural load

As the lateral load increased, (a) a larger lift of the upper panel developed, (b) a smaller compressive deformation of the drypack was observed, (c) the axis of rotation moved slowly from Bar 2 towards the restraint load (**Figure 10**), (d) the compressive region of the drypack narrowed down, and (e) the stress in Bar 2 transformed from compression to tension. In general, the rotational axis was close to Bar 2.

4. FEASIBILITY EVALUATION

The feasibility of THS as a connection for precast walls was evaluated based on the following assessment criteria:

a. C1: The tensile strength of THS should be at least 25% greater than the specified yield strength of the spliced bars (ACI-318, 2008; AC-133, 2008). Hence, the strength ratio, R_s, should be at least 1.25 (Equation 1).

$$R_s = \frac{f_{u,b1}}{f_{sy}} \geq 1.25 \qquad (1)$$

where $f_{u,b1}$ is the ultimate stress in Bar 1 (N/mm^2), and f_{sy} is the spliced bar's specified yield strength (N/mm^2).

The bond stress, $f_{u,b1}$, was calculated per unit area of the spliced bar, as expressed in Equation 2.

$$f_{u,b1} = \frac{4P_{u,b1}}{\pi {d_b}^2} \qquad (2)$$

where $P_{u,b1}$ is the grouted sleeve's tensile capacity (kN), and d_b is the spliced bar's diameter (mm).

Assuming the axis of rotation was located at Bar 2, the tensile capacity of Bar 1, $P_{u,b1}$, was estimated. $P_{u,b1}$ was considered the pullout force acting on the grouted sleeve. Based on the static equilibrium principle, Equation 3 was derived (**Figure 11**).

$$P_{u,b1} = \frac{P_u H_l - W_w B_l}{B_b} \qquad (3)$$

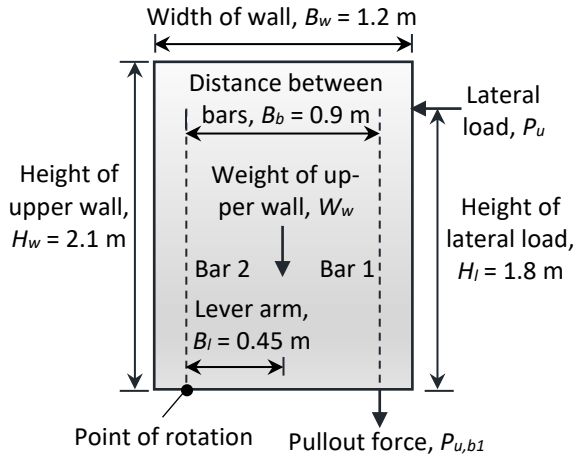

Figure 11. Forces acting on the upper wall

b. C2: The connection should be ductile for survival purposes (ACI-318, 2008; BS8110-1, 1997):

   (i) The drift ratio, R_{df}, should be at least 0.5% (Equation 4) (Hawkins and Ghosh, 2004).

   $$R_{df} = \frac{\delta_u}{H} \geq 0.005 \qquad (4)$$

   where δ_u is the drift of the upper panel at the ultimate state (mm), and H is the height where the lateral load was applied (mm).

   (ii) The ductility ratio, R_d, should be at least 4.0 for a low-moderate seismic region (Equation 5) (Soudki, 1994).

   $$R_d = \frac{\delta_u}{\delta_y} \geq 4.0 \qquad (5)$$

   where δ_u is the ultimate drift of the upper wall (mm), and δ_y is the yield displacement of the upper wall (mm).

c. C3: The bond strength of THS should be greater than the tensile capacity of the spliced bars. Thus, bar fracture failure was preferred.

d. C4: The load capacity of the specimen should be comparable to the control specimen. Thus, the performance ratio, R_p, should be at least 1.0 (Equation 6).

   $$R_p = \frac{P_u}{P_{u,c}} \geq 1.0 \qquad (6)$$

   where P_u is the ultimate capacity of the specimen (kN), and $P_{u,c}$ is the ultimate capacity of the control specimen (kN).

e. C5: The service load should not be too low compared with the ultimate load. Thus, the serviceability ratio, R_{sv}, should be at least 0.75 (Equation 7) (Ling *et al*., 2017).

   $$R_{sv} = \frac{P_{sv}}{P_u} \geq 0.75 \qquad (7)$$

   where P_{sv} is the service load of the specimen, which was considered equal to the yield load, P_y (kN), and P_u is the ultimate capacity of the specimen (kN).

f. C6: The required embedded length of THS should be less than that conventionally lapped in the wall panels. Thus, the length ratio, R_l, should be less than 1.0.

   $$R_l = \frac{l_b}{l_l} \leq 1.0 \qquad (8)$$

   where l_b is the required bar embedded length in the sleeve (mm), and l_l is the required bar lapping length in concrete (mm).

The specimens were evaluated for feasibility in **Table 7**. The specimen that fulfilled all the assessment criteria was considered feasible. Only THS-8 was found feasible. It required at least 175 mm of bar embedded length to meet the requirements. This was equivalent to 11 times the diameter of the spliced bar.

Table 7. Feasibility evaluation of specimen under flexural load

Criteria	C1*[1]			C2(i)*[2]	C2(ii)*[2]	C3*[3]	C4*[2]	C5*[2]		C6*[4]	Score*[5]	Remarks*[6]
	$P_{u,b1}$ (kN)	$f_{u,b1}$ (N/mm^2)	R_s	R_{df}	R_d	Failure mode	R_p	P_{sv} (kN)	R_{sv}	R_l		
Ref.	Eq. 3	Eq. 2	Eq. 1	Eq. 4	Eq. 5	Table 4	Eq. 6	Table 4	Eq. 7	Eq.8		
Req.			≥1.25	≥0.005	≥4.0	F	≥1.0		≥0.75	≤1.0		
THS-2	85.7	426	0.85	0.002	1.06	S	0.62	45.2	1.00	0.16	1/7	N
THS-4	153.3	762	1.52	0.014	7.72	S	1.09	62.7	0.79	0.26	5/7	N
THS-5	139.3	693	1.39	0.012	4.50	S	0.99	61.8	0.86	0.26	5/7	N
THS-6	100.5	500	1.00	0.003	1.43	S	0.73	52.6	1.00	0.26	2/7	N
THS-8	150.1	747	1.49	0.023	10.14	F	1.07	64.0	0.83	0.36	7/7	A

*Note: [1]Dimensions of upper wall, B_w = 1.2 m, H_w = 2.1 m, and T_w = 0.15 m; Unit weight of concrete, γ_c = 25 kN/m^3; $W_w = B_w H_w T_w \gamma_c = 9.45$ kN; B_l = 0.45 m, H_l = 1.8 m, B_b = 0.9 m, d_b = 16 mm, f_{sy} = 500 N/mm^2,
[2]P_y, δ_y, P_u, and δ_u refer to Table 4, $P_{u,c}$ = 72.5 kN, $P_{sy} = P_y$,
[3]F – bar fracture failure, S – bar bond-slip failure
[4]l_b refer to Table 1, $l_l = 30d_b = 480$ mm (concrete grade 40) (Eurocode 2, 2004; Eurocode Applied.Com),
[5]Score = number of criteria fulfilled / total number of criteria
[6]Y – Feasible, N – Not feasible

5. CONCLUSION

In this study, Tapered Head Sleeves (THS) were used to connect precast walls. The specimens were tested with lateral loads until failure.

From the study, the following conclusions are drawn:

a. The upper wall drifted when subjected to the lateral load. The drift was due to the combined effects of the horizontal slip, rocking displacement, cantilever bending deformation, and compressive settlement.
b. The load capacity of the specimen was influenced by the bar embedded length and the sleeve diameter. The ultimate load increased by 71% as the embedded length increased from 75 mm to 175 mm. The ultimate load increased by 50% when the sleeve's diameter decreased from 75 mm to 50 mm.
c. Only THS-8 was found feasible as the connection for precast walls. It required a bar embedded length of 11 times the diameter of the spliced bar.

Notably, this study was only a preliminary exploration. The main purpose was to test the feasibility of a grouted sleeve as a precast wall connection. The study covered two parameters, namely the sleeve diameter and bar embedded length. The other governing factors such as the bar diameter, grout strength, and sleeve thickness were not investigated. Moreover, only one specimen was tested for each configuration. In this study, the control specimen failed prematurely. Thus, the result obtained did not reflect the full capacity of the specimen. This, to some extent, made the findings of this study to be less persuasive. More experimental studies are needed to accurately clarify the working mechanism of the specimen.

ACKNOWLEDGMENT

We thank the financial support of the Construction Industry Research Institute of Malaysia (CREAM) and the Construction Industry Development Board (CIDB) through Research Grant Vot 73713.

REFERENCES

AC-133. (2008). Acceptance criteria for mechanical connector systems for steel reinforcing bars. ICC Evaluation Service, Inc.

ACI-318. (2008). Building code requirements for structural concrete and commentary. American Concrete Institute.

Al-Jelawy, H. M. (2022). Experimental and numerical investigations on monotonic tensile behavior of grouted sleeve couplers with different splicing configurations. Engineering Structures, 265, 114434.

Alias, A., Sapawi, F., Kusbiantoro, A., Zubir, M., & Rahman, A. B. (2014). Performance of Grouted Splice Sleeve Connector under Tensile Load. JOURNAL OF MECHANICAL ENGINEERING AND SCIENCES, 7, 1094–1102.

Alias, A., Zubir, M. A., Shahid, K. A., & RAhman, A. B. A. (2013). Structural Performance of Grouted Sleeve Connectors with and without Transverse Reinforcement for Precast Concrete Structure. Procedia Engineering, 53, 116–123.

ASTM A1034/A. (2005). Standard test methods for testing mechanical splices for steel reinforcing bars. ASTM International.

ASTM E564-06. (2006). Standard practice for static load test for shear resistance of framed walls for building. ASTM International.

Baharuddin, A., Rahman, A., & Hosseini, S. J. A. (2013). Analysis of spiral reinforcement in grouted pipe splice connectors. GRAĐEVINAR, 65(6), 537–546.

BS-EN 1992-1-1:2004. (2004). Eurocode 2: Design of concrete structures - Part 1-1: General rules and rules for buildings. British Standards Institution.

BS8110-1:1997. (1997). Structural use of concrete - Part 1: Code of practice for design and construction BS 8110. British Standards Institution.

Einea, A., Yamane, T., & Tadros, M. K. (1995). Grout-Filled Pipe Splices for Precast Concrete Construction. Precast/Prestressed Concrete Institute Journal, 40, 82–93.

Eurocode Applied.Com. (n.d.). Eurocode 2: Table of reinforcement anchorage length and lap length. Retrieved November 16, 2022, from https://eurocodeapplied.com/design/en1992/anchorage-and-lap-length-table

Haber, Z., Saiidi, M., & Sanders, D. (2015). Behavior and Simplified Modeling of Mechanical Reinforcing Bar Splices. Aci Structural Journal, 112. https://doi.org/10.14359/51687455

Hawkins, N. (2004). Acceptance Criteria for Special Precast Concrete Structural Walls Based on Validation Testing. PCI Journal, 49. https://doi.org/10.15554/pcij.09012004.78.92

Henin, E., & Morcous, G. (2015). Non-proprietary bar splice sleeve for precast concrete construction. Engineering Structures, 83, 154–162.

Henry, R. E. U. and R. L. (n.d.). Influence of Normal Pressure on Bond Strength. ACI Journal Proceedings, 62(5). https://doi.org/10.14359/7711

Hosseini, S. J. A., & Rahman, A. B. A. (2016). Effects of spiral confinement to the bond behavior of deformed reinforcement bars subjected to axial tension. Engineering Structures, 112, 1–13. https://doi.org/https://doi.org/10.1016/j.engstruct.2015.12.038

Hosseini, S. J. A., Rahman, A. B. A., Osman, M. H., Saim, A., & Adnan, A. (2015). Bond behavior of spirally confined splice of deformed bars in grout. Construction and Building Materials, 80, 180–194. https://doi.org/https://doi.org/10.1016/j.conbuildmat.2014.12.097

Huang, Z., Yang, Y., Zhang, J., Ma, S., & Cao, C. (2023). Experimental study on the tensile performance of a large-diameter UHPC grouted sleeve with thread. Engineering Structures, 294, 116707. https://doi.org/https://doi.org/10.1016/j.engstruct.2023.116707

Koushfar, K., Rahman, A., Ahmad, Y., & Osman, M. (2014). Bond behavior of the reinforcement bar in glass fiber-reinforced polymer connector. Gradjevinar, 66, 301–310.

Li, Y., Zhang, L., Zhang, Q., He, X., Wang, J., & Su, Y. (2022). Anchorage behavior of grouting sleeves under uniaxial and cyclic loading-A comparative study of the internal structure of sleeves. Journal of Building Engineering, 49, 104057.

Lin, F., & Zhao, P. (2020). Behavior of Grouted Sleeve Splice for Steel Profile under Tensile Loadings. Materials, 13, 2037. https://doi.org/10.3390/ma13092037

Ling, J. H. (2011). Behaviour of Grouted Splice Connections in Precast Concrete Wall Subjected to Ten-sile, Shear and Flexural Loads. In Universiti Teknologi Malaysia.

Ling, J. H., Abd. Rahman, A. B., & Ibrahim, I. S. (2014). Feasibility study of grouted splice connector under tensile load. Construction and Building Materials, 50, 530–539.

Ling, J. H., Abd. Rahman, A. B., Ibrahim, I. S., & Abdul Hamid, Z. (2012). Behaviour of grouted pipe splice under incremental tensile load. Construction and Building Materials, 33, 90–98. https://doi.org/https://doi.org/10.1016/j.conbuildmat.2012.02.001

Ling, J. H., Abd. Rahman, A. B., Ibrahim, I. S., & Abdul Hamid, Z. (2016). Tensile capacity of grouted splice sleeves. Engineering Structures, 111, 285–296.

Ling, J. H., Rahman, A. B. A., & Ibrahim, I. S. (2022). Deformation Behavior of Grouted Sleeve Wall Connector Under Shear Load in Precast Process of Concrete Wall. In Indonesian Journal of Computing, Engineering, and Design (IJoCED) (Vol. 4, Issues 2 SE-Articles, pp. 1–14). https://doi.org/10.35806/ijoced.v4i2.263

Ling, J. H., Rahman, A., Ibrahim, I., & Abd. Hamid, Z. (2017). An Experimental Study of Welded Bar Sleeve Wall Panel Connection under Tensile, Shear, and Flexural Loads. International Journal of Concrete Structures and Materials, 11.

Ling, J. H., Rahman, A., Mirasa, A. K., & Hamid, Z. (2008). Performance of CS-sleeve under direct tensile load: Part i - Failure modes. Malaysian J Civil Eng, 20.

Lu, Z., Huang, J., Li, Y., Dai, S., Peng, Z., Liu, X., & Zhang, M. (2019). Mechanical behaviour of grouted sleeve splice under uniaxial tensile loading. Engineering Structures, 186, 421–435. https://doi.org/https://doi.org/10.1016/j.engstruct.2019.02.033

Ma, G., Qin, C., Hwang, H.-J., & Zhou, Z. (2023). Data-driven models for predicting tensile load capacity and failure mode of grouted splice sleeve connection. Engineering Structures, 289, 116236. https://doi.org/https://doi.org/10.1016/j.engstruct.2023.116236

Moosavi, M., Jafari, A., & Khosravi, A. (2005). Bond of cement grouted reinforcing bars under constant radial pressure. Cement and Concrete Composites, 27(1), 103–109.

Rahman, A. B., Ling, J. H., Ibrahim, I., & Abd. Hamid, Z. (2010). Performance of grouted sleeve connectors subjected to incremental tensile loads. Malaysian Constr Res J (MCRJ), 6, 39–55.

Sayadi, A. A., Abd. Rahman, A. B., Sayadi, A., Bahmani, M., & Shahryari, L. (2015). Effective of elastic and inelastic zone on behavior of glass fiber reinforced polymer splice sleeve. Construction and Building Materials, 80, 38–47.

Sayadi, A. A., Rahman, A. B. A., Jumaat, M. Z. Bin, Johnson Alengaram, U., & Ahmad, S. (2014). The relationship between interlocking mechanism and bond strength in elastic and inelastic segment of splice sleeve. Construction and Building Materials, 55, 227–237.

Seo, S.-Y., Nam, B.-R., & Kim, S.-K. (2016). Tensile strength of the grout-filled head-splice-sleeve. Construction and Building Materials, 124, 155–166.

Soudki, K. A. (1994). Behaviour of horizontal connections for precast concrete load-bearing shear wall pan-els subjected to reversed cyclic deformations. University of Manitoba.

Sun, Y., Sun, Z., Yao, L., Wei, Y., & Wu, G. (2021). Bond performance between SFCBs and grouted sleeves for precast concrete structures. Advances in Structural Engineering, 24(13), 2857–2869. https://doi.org/10.1177/13694332211001505

Tastani, S., & Pantazopoulou, S. (2002). EXPERIMENTAL EVALUATION OF THE DIRECT TENSION - PULLOUT BOND TEST.

Tibbetts, A., Oliva, M., & Bank, L. (2009). Durable Fiber Reinforced Polymer Bar Splice Connections for Precast Concrete Structures. Composites & Polycon, 15–17.

Tullini, N., & Minghini, F. (2016). Grouted sleeve connections used in precast reinforced concrete construction – Experimental investigation of a column-to-column joint. Engineering Structures, 127, 784–803.

Wang, Z., Zhu, J., Wang, J., Zhao, G., Sun, S., & Zhang, J. (2021). Experimental study on a novel UHPC grout-filled pipe sleeve with mechanical interlocking for large-diameter deformed bars. Engineering Structures, 226, 111358.

Xu, T., Li, Q., Zhao, R., Ding, J., & Zhan, Y. (2019). On the early-age bond-slip behavior of an eccentric bar embedded in a grouted sleeve. Engineering Structures, 190, 160–170. https://doi.org/https://doi.org/10.1016/j.engstruct.2019.04.020

Zheng, Y., Guo, Z., Guan, D., & Zhang, X. (2018). Parametric study on a novel grouted rolling pipe splice for precast concrete construction. Construction and Building Materials, 166, 452–463. https://doi.org/https://doi.org/10.1016/j.conbuildmat.2018.01.182